AIAA JOURNAL
Vol. 42, No. 9, September 2004

Effect of Oscillations on Airfoils in Close Proximity to the Ground

Yair Moryossef* and Yuval Levy†
Technion—Israel Institute of Technology, 32000 Haifa, Israel

Numerical simulations are conducted to study the flowfield about oscillating airfoils in close proximity to the ground. Inviscid and viscous turbulent flow simulations are conducted by the use of a full Navier–Stokes code and a one-equation, topology-free turbulence model. Comparison of results from fixed airfoil simulations suggest that inviscid flow assumptions are valid only for a moderate to high distances from the ground. Viscous flow simulations reaffirm the so-called down-force reduction phenomenon. The viscous flow simulations about an oscillating airfoil show that at close proximity to the ground and low reduced frequencies, viscous effects are dominant, whereas at high reduced frequencies the behavior resembles that of inviscid flows. Inviscid flow simulations about an oscillating airfoil show that as the ground clearance decreases, the total thrust that is created due to the airfoil motion increases. The results point to an approximated relation between the thrust and the reduced frequency. It is also shown that the lift phase lag behavior concerning the flow about an oscillating airfoil in close proximity to the ground is different in nature than the classical behavior of oscillating airfoils in freestream. Consequently, the amplitude of the lift force approaches a nonzero value for reduced frequencies approaching zero.

Nomenclature

$C(k)$	=	lift deficiency function
C_l	=	lift coefficient
C_{l_α}	=	lift coefficient slope
$C_{l_{\alpha_e}}$	=	effective lift coefficient slope
C_p	=	pressure coefficient
c	=	airfoil chord
H	=	ride height
h	=	initial ride height
h_0	=	amplitude of motion
k	=	reduced frequency, $\omega c/2U_\infty$
T	=	total thrust, $-\bar{X}$
t	=	time
U_∞	=	freestream velocity
X	=	streamwise force
$\bar{X}$	=	average streamwise force
α	=	angle of attack
α_e	=	effective angle of attack
α_{l_0}	=	zero lift angle of attack
ω	=	angular frequency

Subscripts

aig	=	airfoil in ground effect
aog	=	airfoil out of ground effect

Introduction

AERODYNAMIC research of open-wheel race cars is an area of increasing interest and growing investment, particularly regarding Formula One race cars. The performance of such high-speed ground vehicles may be considerably increased by application of an aerodynamic down-force (negative lift). Down-force can be created by shaping the vehicle body and by the addition of front and rear wings. Race car wings are, therefore, highly cambered with the suction side down. The front and rear wings of racing cars are composed of several wing elements with end plates. The front wing is mounted on the nose of the car in close proximity to the ground and, based on varying regulations, the ground clearance is typically between 30 and 50% of the wing chord. Therefore, race car wings are greatly affected by the ground presence.

The effect of the ground can be modeled in various ways. One method is the method of images, where the ground is simulated by reflection and the effect is known as the classical ground effect. Such methods are also utilized concerning the flow about birds' flapping wings.[1] Another way to model the ground is by direct imposition of the ground presence by introduction of a solid boundary, for example, a flat board placed underneath the wing. Previous studies show that when an airfoil is placed at close proximity to the ground, the ground effect becomes more significant, and an appropriate model of a moving ground is necessary to achieve a realistic description of the flowfield.[2] As will be shown later, when the ground clearance decreases below a certain height, viscous effects cannot be neglected, and the effect of the ground is termed in the current work extreme ground effect.

Past studies concerning the flow about wings in ground effect may be divided into two main types, fixed wings and oscillating wings. In this study, a fixed wing in ground effect refers to a wing located at a fixed height above the ground. An oscillating wing in ground effect refers to a wing that oscillates about a specific average height above the ground. The interest in the effect of the oscillations on wings in close proximity to the ground arises because the front wing of an open-wheel race car experiences oscillations due to the road conditions.

To date, all of the experimental work concerning wings in close proximity to the ground concerned fixed wings only. Numerical studies have been utilized to study both fixed and oscillating wing flows. Most fixed wing simulations have been conducted by solution of the Navier–Stokes equations, whereas most simulations of oscillating wings have been conducted by the use of vortex lattice methods.[2]

Knowles et al.[3] experimentally investigated the flow about an inverted (suction surface down) fixed wing in ground effect. In an effort to better account for the road conditions, they were the first to use a moving belt to obtain a more realistic flow. Forces and moments were measured about a wing based on the GA(W)-1 airfoil with its suction surface located between 0.12 and 1.0 chords above the moving belt. They showed that decreasing ground clearance generally increased the lift curve slope, the drag, and the pitching moment.

Ranzenbach and Barlow[4–6] conducted a series of studies concerning the flow about fixed airfoils in ground effect. Their studies included experiments and numerical simulations of the flow about

Received 10 November 2003; revision received 8 March 2004; accepted for publication 19 March 2004.

*Graduate Student, Faculty of Aerospace Engineering; yairm@bellini.technion.ac.il.

†Senior Lecturer, Faculty of Aerospace Engineering; yuval@bellini.technion.ac.il. Senior Member AIAA.

various single-element inverted airfoils, at different fixed heights from the ground, at a single angle of attack. The experiments did not include a moving belt, whereas the numerical simulations were conducted by the use of RANS simulations,[7] with and without moving ground boundary conditions. They found that the down-force was increased as the distance from the ground decreased. However, at a height of about 0.1 chord from the ground, the down-force reached a maximum, and below this height the down-force dropped sharply. In addition, they showed that as the airfoil ride height decreased, the drag force increased, even at heights where the down-force decreased. They argued that the down-force reduction phenomenon is due to the merge of the ground boundary layer with the airfoil wake.

Zerihan and Zhang[8,9] experimentally studied a single-element, inverted, fixed wing with end plates. The wing section was the main element of the Tyrrell 026 Formula One race car front wing. To simulate the moving ground, the experiment was performed with a moving belt, and the wing was tested with free and fixed transition. Similar to the results presented by Ranzenbach and Barlow, they showed that when the distance between the lowest point of the suction surface and the ground dropped below 10% of the chord, the trend of increasing down-force changed to a decreasing down-force.

Zerihan and Zhang[8] claimed that the physical effect of the ground was to constrain the flow between the suction surface of the wing and the ground. This caused an acceleration of the flow on the suction surface and a subsequent pressure reduction and, hence, a down-force. As the wing ride height decreased, the flow acceleration increased, generating a higher down-force. However, the increasing flow acceleration eventually caused an adverse pressure gradient, which in turn caused the flow to separate. Furthermore, below a certain ride height, the large separated region resulted in a trend reversal, that is, a decreasing down-force with decreasing ride height. In contrast to Ranzenbach and Barlow, Zerihan and Zhang concluded that the flow separation is the origin of the down-force reduction phenomenon. Zerihan and Zhang[10] also conducted a numerical study of the two-dimensional flow about the Tyrrell 026 airfoil and compared their results with the results presented in Ref. 9. They reported a good agreement between the results.

As just mentioned, most of the numerical investigations concerning oscillating wings in ground effect have been conducted by the use of vortex lattice methods. (See the work by Barber et al.[2] for a comprehensive reference list.) In these methods, the ground effect is modeled by reflection. However, according to Barber et al. image methods in conjunction with vortex lattice methods cannot provide a sufficiently accurate representation of the flow about wings in close proximity to the ground. Moreover, Barber et al. showed that for such flows, a moving ground is also necessary to obtain a realistic flow simulation.

The present work utilizes computational fluid dynamics simulations to study the flow about a fixed airfoil and a heaving oscillating airfoil in ground effect at a single incidence. The flow simulations are conducted about a single-element airfoil that is based on the main element of the Tyrrell 026 Formula One race car front wing. Figure 1 shows a schematic description of the Tyrrell 026 wing section in ground effect. The height from the ground is defined as the vertical distance from the ground to the lowest point of the airfoil and is denoted by H. The oscillating airfoil, performing a heaving motion, oscillates about an initial height h with an amplitude h_0. The fixed airfoil simulations are conducted for heights ranging between $H/c = 0.08$ and $H/c = 0.7$. The simulations include both inviscid flow simulations and viscous turbulent flow simulations.

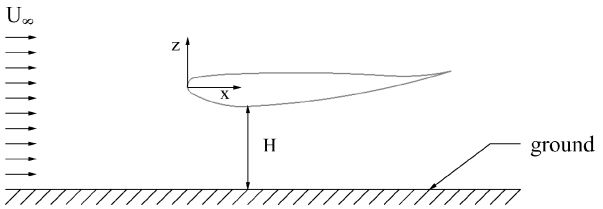

Fig. 1 Side view of the Tyrrell 026 wing section in ground effect.

The oscillating airfoil simulations are conducted for flows in and out of ground effect. To better account for the extreme ground effect flow conditions, viscous flow simulations, as well as inviscid flow simulations, are also conducted. In addition, comparison between viscous and inviscid flow simulations allows elucidation of the various mechanisms concerning such flows. The oscillatory simulations in ground effect are conducted about normalized heights ranging between $h/c = 0.313$ and $h/c = 0.7$. The unsteady heaving motion is a sinusoidal motion with reduced frequencies ranging from $k = 0.06$ to $k = 1.3$, and a constant amplitude, $h_0 = 0.1c$. The reduced frequency is defined as $k = \omega c/2U_\infty$. For each of the cases, the solution is restarted from a converged solution of the corresponding fixed airfoil case. The flow conditions are as follows: The freestream Mach number is set to $M_\infty = 0.09$, the angle of attack to $\alpha = -3.2$ deg, and, for the viscous turbulent flow, the Reynolds number is set to $Re = 4.6 \times 10^5$.

Numerical Scheme

The current study is conducted by the use of the EZNSS flow solver, developed by Levy.[11] The code is an Euler/Navier–Stokes solver with second-order spatial and temporal accuracy. The code is based on finite differences, and it utilizes the formulation of the Navier–Stokes equations in curvilinear coordinates as follows:

$$\frac{\partial \hat{\boldsymbol{Q}}}{\partial \tau} + \frac{\partial \hat{\boldsymbol{E}}}{\partial \xi} + \frac{\partial \hat{\boldsymbol{F}}}{\partial \eta} + \frac{\partial \hat{\boldsymbol{G}}}{\partial \zeta} = \frac{1}{Re}\left(\frac{\partial \hat{\boldsymbol{E}}_v}{\partial \xi} + \frac{\partial \hat{\boldsymbol{F}}_v}{\partial \eta} + \frac{\partial \hat{\boldsymbol{G}}_v}{\partial \zeta}\right) \quad (1)$$

The vector $\hat{\boldsymbol{Q}}$ is the vector of conserved mass, momentum, and energy. The vectors $\hat{\boldsymbol{E}}$, $\hat{\boldsymbol{F}}$, and $\hat{\boldsymbol{G}}$ represent the inviscid rotated fluxes, whereas $\hat{\boldsymbol{E}}_v$, $\hat{\boldsymbol{F}}_v$, and $\hat{\boldsymbol{G}}_v$ represent the viscous flux vectors. The code provides the choice between various implicit algorithms, among which are the Beam and Warming[12] algorithm and the flux-vector splitting algorithm reported by Steger and Warming.[13] In the current work, only the Beam and Warming algorithm is used. The code is capable of simulating the time-accurate flow about dynamically deforming geometries, and it is fully parallelized. Grid generation and intergrid connectivity are handled via the Chimera approach.[14] An outer mesh is generated and extended to include fully the meshes of all of the geometry components. For example, in the current work, the outer mesh is the freestream and road conditions mesh, whereas a second mesh is generated for the airfoil. The holes that the airfoil introduces into the freestream mesh and the boundaries of the meshes and the holes are handled by the use of interpolations as in the Chimera approach.

An important feature of the code is the ability to control the size of the hole introduced by the airfoil. The close proximity to the ground reduces numerical stability limits and cutting larger holes allows provision of interpolation points from small gradient regions. Control of the hole size was found to be pivotal to the success of the unsteady simulations. The hole generation and the grid connectivity procedures are embedded in the EZNSS code to facilitate the motion of the airfoil.

As mentioned earlier, the computational mesh consists of two grids, one for the freestream and road conditions (hence forth called the outer grid) and one for the airfoil. Two different meshes are utilized, one for the inviscid flow simulations and one for the viscous flow simulations. The results presented in this work correspond to the following mesh dimensions. For the inviscid flow simulations, the outer grid consists of 100 points in the streamwise direction, and 125 points in the vertical direction. The airfoil grid is a C-type mesh, and it consists of 173 points in the circumferential direction (99 points on the airfoil surface) and 41 points normal to the airfoil surface.

For the viscous flow simulations, the outer grid consists of 170 points in the streamwise direction and 150 points in the vertical direction. The airfoil grid consists of 467 points in the circumferential direction (317 points on the airfoil surface) and 70 points normal to the airfoil surface. The first grid point above all solid walls is set to obtain a value of $y^+ \approx 1$. The dimensions of the respective meshes were set based on extensive grid resolution studies. For complete details, see Ref. 15.

Turbulence Model

Numerical simulations of turbulent flows require the solution of the Reynolds-averaged Navier–Stokes (RANS) equations along with the evaluation of the Reynolds stresses. A one-equation topology-free turbulence model, developed by Goldberg,[16] was adapted and added to the EZNSS flow solver. The model consists of a transport equation for the undamped eddy viscosity (denoted as R), as follows:

$$\rho \frac{DR}{Dt} = \frac{\partial}{\partial x_j}\left[\left(\mu + \frac{\mu_t}{\sigma_R}\right)\frac{\partial R}{\partial x_j}\right] + C_1\rho(RP_k)^{0.5} - (C_3 f_3 - C_2)\rho D \tag{2}$$

The undamped eddy viscosity is defined as

$$R = \mu_t/\rho f_\mu \tag{3}$$

where μ_t is the turbulent viscosity. The production term, denoted by P_k, has the form

$$P_k = \nu_t\left[\left(\frac{\partial U_i}{\partial x_j} + \frac{\partial U_j}{\partial x_i}\right)\frac{\partial U_i}{\partial x_j} - \frac{2}{3}\left(\frac{\partial U_k}{\partial x_k}\right)^2\right] \tag{4}$$

where ν_t is the kinematic eddy viscosity, $\nu_t = \mu_t/\rho$. The destruction term, denoted by D, has the form

$$D = \begin{Bmatrix} \dfrac{\partial R}{\partial x_j}\dfrac{\partial R}{\partial x_j}, & \dfrac{\partial Q}{\partial x_j}\dfrac{\partial R}{\partial x_j} > 0 \\ 0, & \text{otherwise} \end{Bmatrix} \tag{5}$$

where Q is defined by $[(U-U_0)^2 + (V-V_0)^2 + (W-W_0)^2]^{1/2}$. The vector (U_0, V_0, W_0) represents the velocity of the reference frame. The equation is subjected to the following boundary conditions: $R = 0$ at solid walls and $R_\infty \le \nu_\infty$ at freestream (and initial conditions). The constants C_1, C_2, and C_3 and the functions f_μ and f_3, as well as complete details of the model, may be found in Ref. 16.

The fact that the model does not explicitly include a wall distance is significant in its application to flows about airfoils in close proximity to the ground. It allows simulation of flows that are enclosed between two neighboring solid boundaries without the need to determine a different length scale for each boundary layer. Moreover, in certain cases, where the boundary layer developed on the ground may merge with that developed on the airfoil, the use of such a turbulence model provides a significant advantage.

Boundary Conditions

The boundary conditions are specified to simulate the flow about an airfoil in ground effect. Figure 2a shows a schematic description of the outer grid boundaries. Freestream conditions are given at the upstream and top boundaries of the outer grid, and a zeroth-order extrapolation is employed at the downstream boundary. For inviscid flow, an impermeable adiabatic wall boundary condition is applied at the bottom boundary, namely, the ground. The hole boundary is updated by interpolation.

Figure 2b shows a schematic description of the airfoil grid boundaries. All outer boundaries are updated by interpolation. For inviscid flow, an impermeable adiabatic wall boundary condition is applied at the airfoil surface. Along the wake, an average-type cut condition is employed.

The boundary conditions for the viscous turbulent flow simulations are similar, except for the walls where a no-slip adiabatic wall boundary condition is applied. The bottom boundary of the outer grid, namely, the ground, is moving in the freestream velocity.

Fixed Airfoil Simulations

To provide a basis for comparison and as a part of code validation, fixed airfoil simulations are conducted and the results are compared with the experimental results presented by Zerihan and Zhang.[9] The airfoil in their experiment features a finite trailing edge corresponding to a 0.7% chord length. In the current work, the trailing edge is sharp. Note that this may also change the exact definition of the incidence angle. Consequently, slight differences in the results may be caused by the differences between the models.

Figure 3 shows the variation of the lift coefficient as a function of normalized distance from the ground for inviscid and viscous

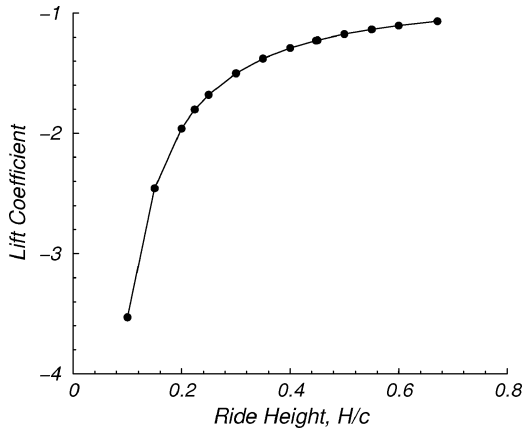

a) Inviscid flow

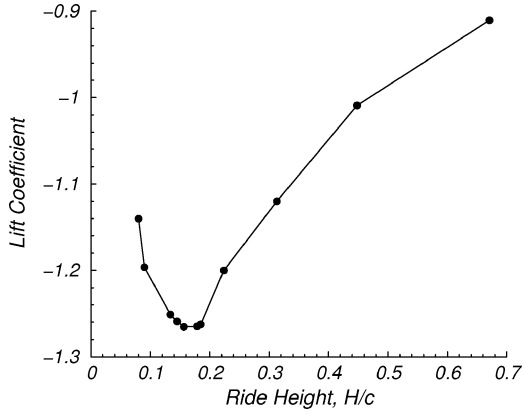

b) Viscous flow

Fig. 3 Lift coefficient variation with ride height.

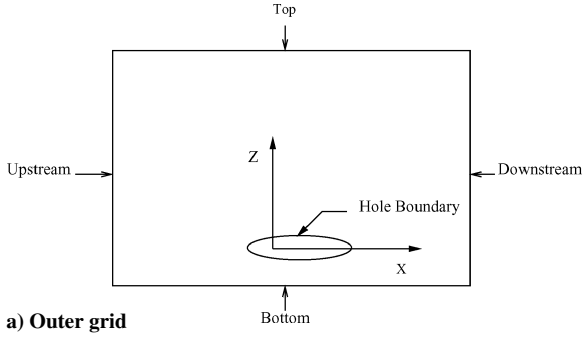

a) Outer grid

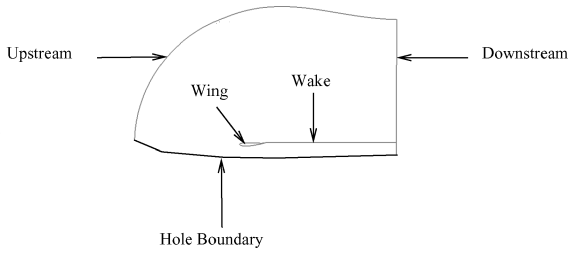

b) Wing grid

Fig. 2 Outer and airfoil grid boundary conditions.

flows. As expected, the results show that there is a significant difference between inviscid and viscous flows in ground effect. For the inviscid flow the down-force increases with decreasing airfoil ride height and the down-force slope continuously increases as the airfoil approaches the ground. On the other hand, for viscous flow, the down-force increases with reducing ride heights, where at a ride height of $H/c = 0.15$ it reaches a maximum of $C_l = -1.26$. Lower than this ride height, there is a reduction in the down-force, and at a ride height of $H/c = 0.08$ the corresponding down-force is $C_l = -1.14$. The sharp loss of down-force after the ride height where the maximum is obtained resembles the behavior of the lift about an airfoil at an angle of attack. Therefore, this certain ride height may be considered the ride height where the airfoil stalls. Furthermore, one can associate an effective angle of attack to each ride height; thus, a reduction in ride heights corresponds to an increase in the effective angle of attack. At relatively high distances, a decrease in the ride height increases the down force. At smaller distances, a decrease in the ride height causes a higher adverse pressure gradient, which leads to flow separation and to the eventual stall of the airfoil. Similar to the classical stall of airfoils, this airfoil stall is also accompanied by a sharp drag increase.

On the other hand, the behavior exhibited by the inviscid flow simulations is expected. With the absence of viscosity, the decreasing ground clearance causes an increasing Venturi effect. As the area ratio increases, the flow accelerates, resulting in a lower pressure and a higher down force. The results presented in Fig. 3 suggest that the inviscid flow approximation is valid only up to a certain distance from the ground.

To further study the differences between the inviscid and viscous flows, the surface pressure of the respective results are compared. Figure 4 shows a comparison of the surface pressure coefficient between the experimental results[9] and the results from the numerical simulations of viscous and inviscid flows. At a normalized ride height of $H/c = 0.671$ (Fig. 4a), there is an excellent agreement between the experimental and computational viscous flow results. There is a small deviation between the experimental results and the results from the inviscid flow simulations. The differences are extremely small for the pressure surface side whereas they are noticeable for the suction surface side. Yet these differences are relatively small because they show that, at this height, the assumption of a thin, mostly attached boundary layer is reasonable.

At a lower ride height, $H/c = 0.448$ (Fig. 4b), the agreement between the experimental results and the results from the viscous flow simulations remains excellent. At this height, the deviation of the inviscid flow results from the experimental results increases, especially on the suction surface. Still, to a certain extent, the inviscid flow simulation results are acceptable. As the ride height decreases further (Fig. 4c and 4d), the agreement between the experimental results and the results from the viscous flow simulations are good. However, the results from the inviscid flow simulations show a very poor agreement on the suction surface. This means that the inviscid flow simulation assumption does not hold at these heights.

The results presented earlier show that the viscous effects may be neglected for airfoil heights above approximately 50% airfoil chord, where the assumption of inviscid flow is valid. Below that height, the assumption of inviscid flow is incorrect, and the inviscid computations fail to predict the experimental pressure coefficient distribution. It is then essential to distinguish between ground effect and extreme ground effect. Extreme ground effect is defined as height of the airfoil from the ground where viscous effects cannot be neglected.

Oscillating Airfoil Simulations

The flow about oscillating airfoils in freestream exhibits a wide variety of interesting phenomena. The average lift equals the lift

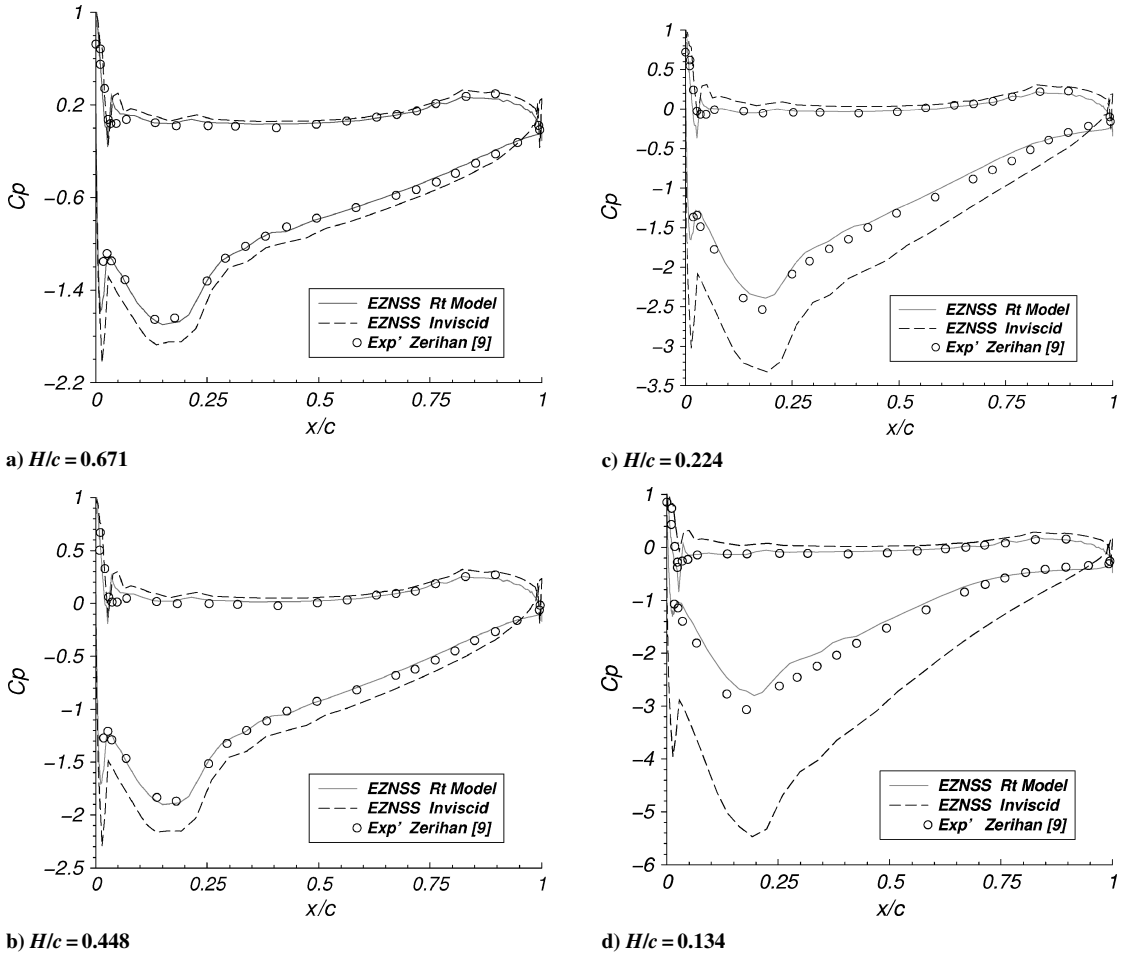

a) $H/c = 0.671$ c) $H/c = 0.224$

b) $H/c = 0.448$ d) $H/c = 0.134$

Fig. 4 Surface pressure coefficient; comparison of experimental[9] and computational results.

of a fixed airfoil because there is no preferred direction. The amplitude of the lift oscillations increases as the oscillating frequency increases.[17] However, the average streamwise force does not equal the drag force acting on a fixed airfoil. As will be shown later, above a certain oscillation frequency there is a forward pointing average streamwise force. In the current work, the instantaneous streamwise force is termed drag when it is positive (backward pointing) and is termed thrust when it is negative. From classical theory, it is known that the amplitude of the streamwise force also increases as the oscillating frequency increases.[18] For a comprehensive review concerning the aerodynamics of flapping wings in freestream, see the work of Rozhdestvensky and Ryzhov.[19]

The ability of a sinusoidally plunging airfoil in inviscid flow to produce thrust is known as the Knoller[20]–Betz[21] or Katzmayr[22] effect. Garrick[18] applied Theodorsen's[17] oscillatory flat-plate theory to determine the thrust and showed that, for a heaving motion, the thrust is proportional to $k^2|C(k)|^2$, where k is the reduced frequency and $C(k)$ is the lift deficiency function.

The behavior of the lift of oscillating airfoils in ground effect is different by nature than that of oscillating airfoils in freestream (henceforth termed out of ground effect). The proximity to the ground causes a different behavior between the upper and lower surfaces, resulting in an average lift that is different than the lift of a fixed airfoil. Furthermore, as is shown in the preceding section, in extreme ground effect, viscous effects cannot be neglected. Therefore, although most of the phenomena associated with oscillating airfoils are considered inviscid, viscous flow simulations of oscillating airfoils in ground effect are conducted.

Viscous Flow Simulations

A series of viscous flow simulations is conducted at three ride heights, $h = 0.313c$, $h = 0.448c$, and $h = 0.671c$ and six reduced frequencies ranging from $k = 0.17$ to $k = 1.3$. The oscillation amplitude in all cases is $h_0 = 0.1c$. For each of the oscillating flow airfoil cases, the flow is restarted from a converged solution of the flow about a fixed airfoil. Figures 5 and 6 show the time history of two cycles of the lift coefficient and the streamwise force coefficient of the airfoil for one representative ride height and one reduced frequency. To avoid the inclusion of transient effects in the analysis, the first cycle of the oscillation following the restart is omitted. It is clear from Figs. 5 and 6 that the lift coefficient has one dominant frequency where the drag coefficient exhibits at least two noticeable frequencies. It is also clear that, for a part of the cycle, the airfoil experiences a forward acting force, that is, thrust (Fig. 6).

To further analyze the unsteady response of the flow to the sinusoidal heaving motion, fast Fourier transforms (FFT) are performed on the results. Figures 7 and 8 show power spectral density plots for two representative ride heights and a single reduced frequency ($k = 0.7$). An important observation from the FFT analysis of the

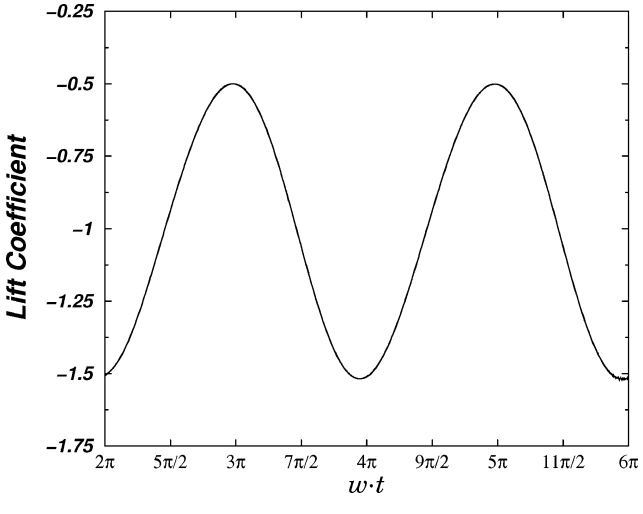

Fig. 5 Lift coefficient time history in ground effect.

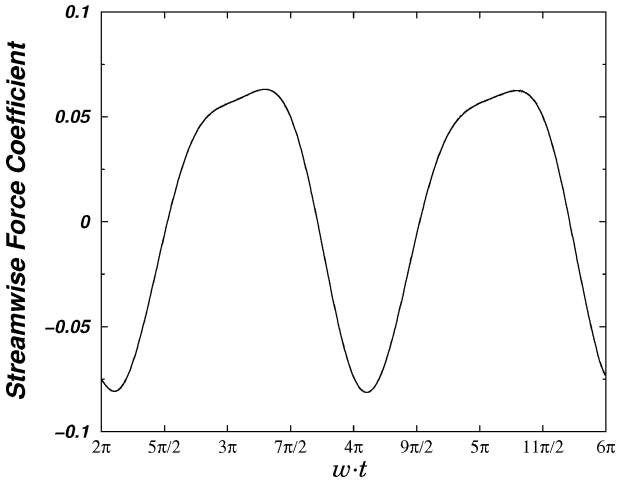

Fig. 6 Streamwise force coefficient time history in ground effect.

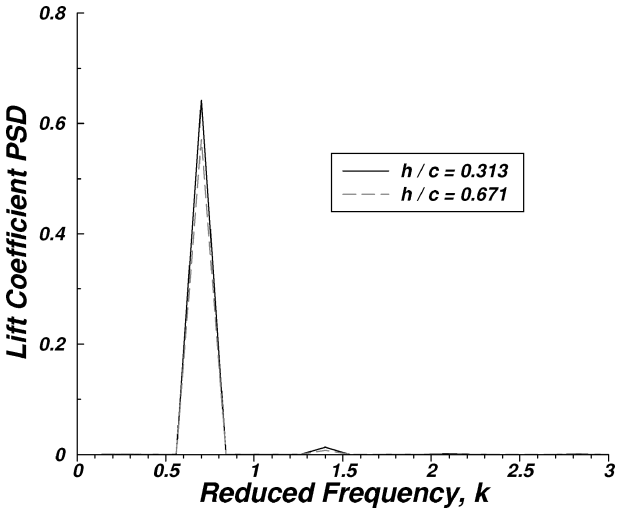

Fig. 7 FFT analysis of the lift coefficient, $k = 0.7$.

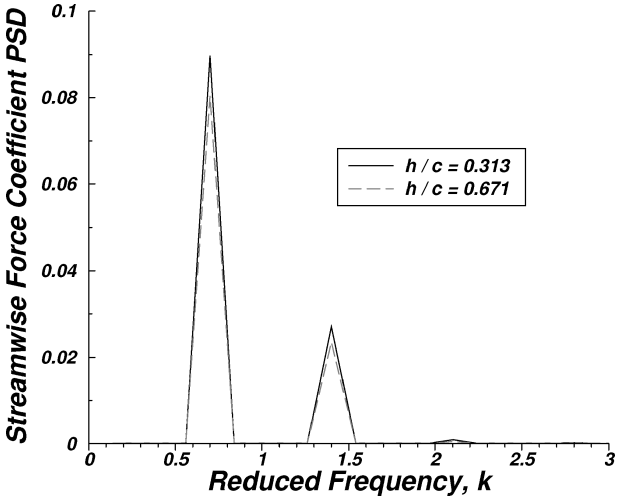

Fig. 8 FFT analysis of the streamwise force coefficient, $k = 0.7$.

lift response (Fig. 7) is that the second mode and higher modes are negligible compared to the first mode. In contrast, the streamwise force response shows that the second mode is smaller than the first mode, but that they are of the same order, especially at high reduced frequencies (Fig. 8). Note, both first and second modes of the streamwise force are caused by linear effects.

Figure 9 shows plots of the first mode lift coefficient vs the reduced frequency k for the three ride heights considered. Figure 10

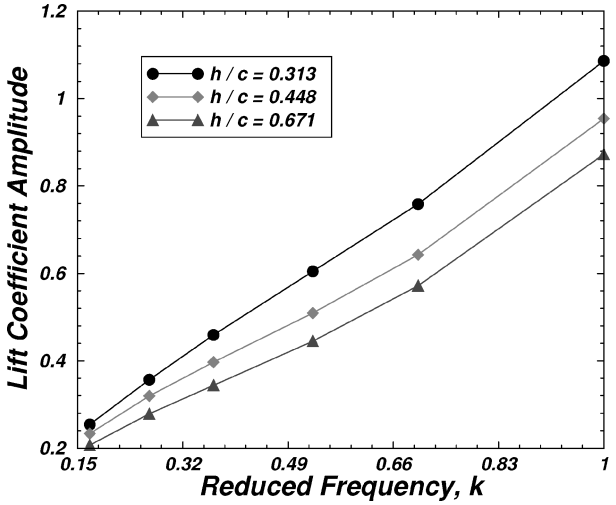

Fig. 9 First mode lift coefficient amplitude in ground effect.

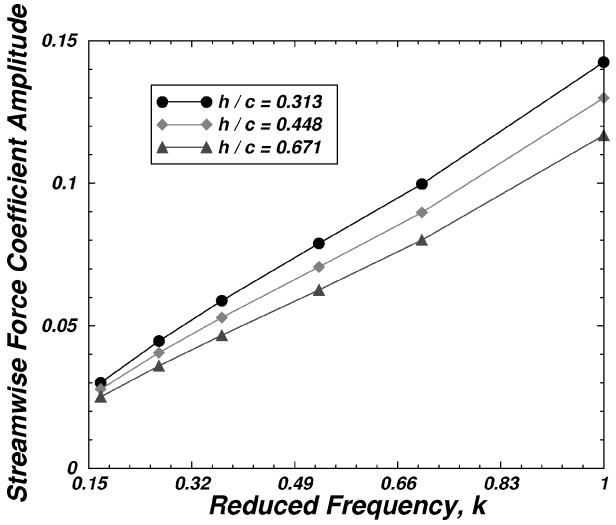

Fig. 10 First mode streamwise force coefficient amplitude in ground effect.

shows the plots of the first mode of the streamwise force coefficient. The results show that the amplitude of both the lift and the streamwise force increase as the reduced frequency is increased. The results also show that the amplitudes increase as the average ride height decreases.

Because the lift force acting on the oscillating airfoil under the conditions considered in the current work is negative throughout the cycle, it is clear that the average lift force is negative. However, as will be shown later, the average streamwise force may be positive or negative, depending on the ride height and on the reduced frequency. Figure 11 shows the average streamwise force of one cycle. The average force is evaluated by integration of one cycle, as follows:

$$\bar{X} = \frac{w}{2\pi} \int_0^{\frac{2\pi}{w}} X \cdot \mathrm{d}t \tag{6}$$

As can be seen from Fig. 11, above a certain frequency, the overall thrust through one cycle is higher than the overall drag; therefore, $\bar{X}$ is negative. At small frequencies, the overall drag is higher, and the average streamwise force $\bar{X}$ is positive. An interesting phenomenon reflected in Fig. 11 is that at low frequencies, an increase in the reduced frequency increases the average streamwise force. This is true up to a certain frequency that depends on the ride height. From that point on, an increase in the frequency reduces the average streamwise force, and, at a certain frequency, the streamwise force becomes negative. In other words, at low frequencies the average streamwise force is drag, whereas at higher frequencies the average streamwise force is thrust. Furthermore, at low frequencies, where the airfoil motion can be considered a quasi-static motion, the streamwise force (positive in this regime) is higher at lower ride heights, consistent with the results from fixed airfoil simulations. In contrast, at high frequencies, there is a trend reversal where the streamwise force is lower (negative in this regime) for lower ride heights, namely, higher overall thrust. Furthermore, at sufficiently high reduced frequencies, the total thrust is dominated by the oscillatory motion. (See the curve crossover in Fig. 11.)

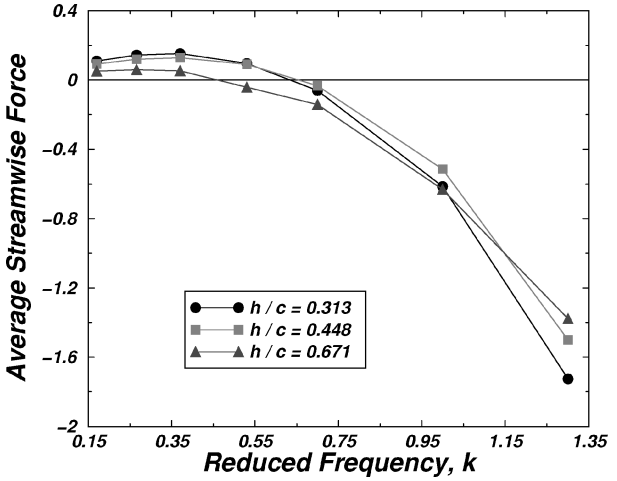

Fig. 11 Average streamwise force in ground effect.

The interesting phenomena exhibited in Fig. 11 can be explained as follows. At low reduced frequencies, the heaving motion produces very little thrust, whereas the motion increases the pressure and friction drag. Therefore, an increase in the frequency results in increased drag, and the higher drag force is obtained at lower ride heights. At high reduced frequencies, the heaving motion becomes more dominant and higher thrust is generated at lower ride heights. As mentioned earlier, the thrust generated by an oscillatory heave motion is the result of an inviscid flow phenomenon. The results presented in this section do not provide the means to isolate the effect of the oscillatory heaving motion. This is because the streamwise force contains the results of multiple effects such as the effect of the heaving motion and viscous effects such as friction drag. Therefore, a series of inviscid flow simulations is conducted.

Inviscid Flow Simulations

One of the most important aspects concerning the inviscid flow simulations about oscillating airfoils is the applicability of the Kutta condition at the trailing edge. Based on previous work conducted by Satyanarayana and Davis[23] concerning the unsteady Kutta condition, the highest reduced frequency that is used in the current study is $k = 0.7$.

The inviscid flow simulations cover average ride heights ranging from $h = 0.35c$ to $h = 0.7c$. Despite the fact that viscous effects cannot be completely neglected below ride heights of approximately $h = 0.5c$, it is believed that important insight into the fundamental behavior of the flow can be gained when the inviscid simulations are conducted in this regime.

Lift of Oscillating Airfoils in Ground Effect

Figure 12 shows the time history of two cycles of the lift coefficient of the airfoil at five different ride heights for two representative reduced frequencies. Note, the general behavior of the lift coefficient is similar to the behavior in viscous flow. The results presented follow the completion of one cycle of airfoil motion. Similar to the behavior of the lift out of ground effect, an increase in the reduced frequency at a constant ride height increases the lift amplitude. However, in contrast to the case of out of ground effect, the average lift is different than that of the corresponding lift of the fixed airfoil. Examination of each of the cycles at a constant reduced frequency

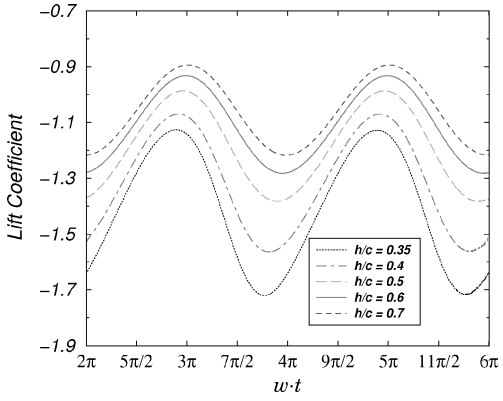

a) $k = 0.1$

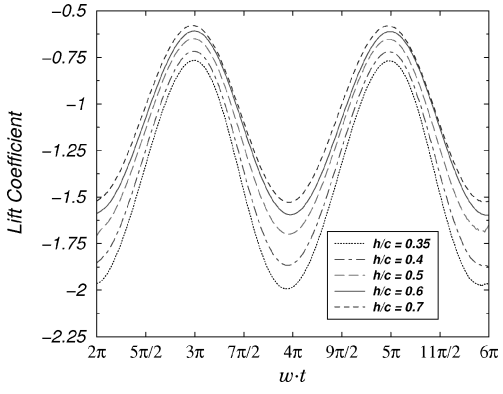

b) $k = 0.53$

Fig. 12 Lift coefficient time history in ground effect.

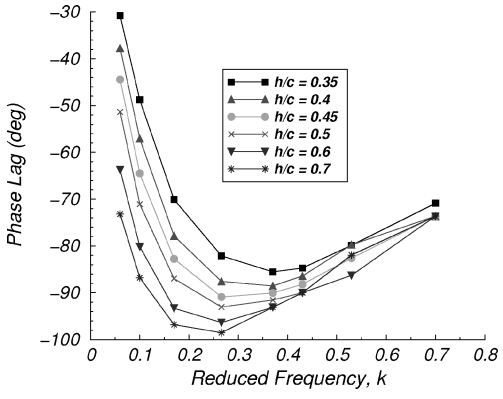

Fig. 13 Lift phase lag in ground effect.

shows that, as the ground clearance is reduced, the upper peak becomes higher (less negative) and the lower peak becomes lower (more negative). The increase in the amplitude is more pronounced concerning the lower peak, which results in an increasing average down-force with decreasing ground clearance.

Figure 13 shows the lift phase lag for different ride heights vs the reduced frequency. The phase lag is evaluated by superimposition of the sinusoidal airfoil motion and the force response and by measurement of the angle between corresponding peaks. A zero phase lag means that the force response exactly follows the airfoil motion. Similar to what is known concerning the flow out of ground effect, the phase lag magnitude increases with increasing reduced frequency to the point where it reaches a maximum. Beyond that point, the phase lag magnitude decreases with increasing reduced frequency. The results presented in Fig. 13 provide a better understanding of the lift behavior of an oscillating airfoil in ground effect. The maximum of the phase lag magnitude occurs at different reduced frequencies for different ride heights. Reduction of the ground clearance moves the maximum point to a higher reduced frequency. Moreover, reduction of the ground clearance decreases the maximum of the phase lag magnitude. Note that the differences between the curves decrease with increasing reduced frequencies. For example, the difference of the phase lag curves between ride heights of $h/c = 0.35$ and $h/c = 0.7$ at the lowest reduced frequency, $k = 0.06$, is approximately 42 deg, whereas for the highest reduced frequency, $k = 0.7$, the difference is approximately only 5 deg.

The phase lag behavior provides insight into another important feature that is revealed by the current work, namely, the unique behavior of the lift about airfoils in ground effect. Classical results of the flow about oscillating airfoils out of ground effect[17] show that as the reduced frequency approaches zero, ($k \rightarrow 0.0$), the phase lag approaches 90 deg. In contrast, the results concerning the phase lag in ground effect suggest that when the reduced frequency approaches zero, the phase lag approaches zero as well. This new observation can be explained when it is noted that for very low reduced frequencies, the airfoil motion can be considered a quasi-static motion. Such motion means that the effect of the wake is negligible and that only the airfoil dynamics is considered. Thus, the instantaneous location of the oscillating airfoil in ground effect corresponds to a different equilibrium condition. This equilibrium condition is analogous to the fixed airfoil in ground effect case. Therefore, the aerodynamic forces follow the airfoil motion and there is no phase lag.

FFTs are performed on the results in this case as well. Similar to the viscous flow case, the second mode and higher modes are negligible compared to the first mode. Figure 14a shows plots of the first mode lift coefficient vs the reduced frequency k for a constant ride height. The lines are approximately parallel, especially at high reduced frequencies. Moreover, at high reduced frequencies, the lines are approximately linear. Following the result of Theodorsen,[17] the curve slope of the lift coefficient amplitude out of ground effect at high reduced frequencies is approximately constant. In contrast, the amplitude variation is nonlinear at low reduced frequencies. This behavior is mainly due to the wake effect.

In terms of potential flow, the wake effect may be presented by the lift deficiency function $C(k)$ (Ref. 17). Theodorsen showed that at

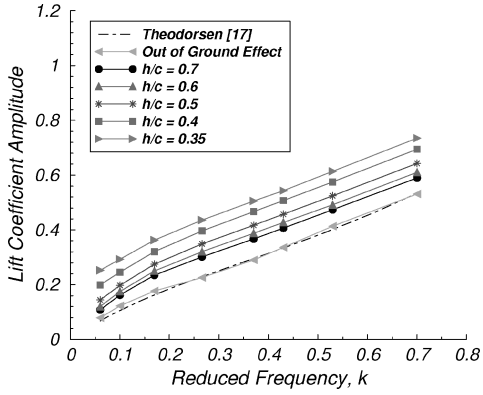

a)

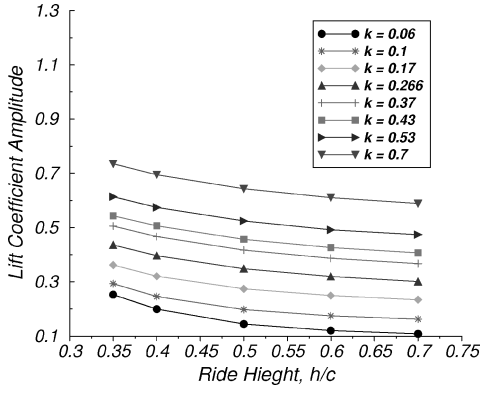

b)

Fig. 14 First mode lift coefficient amplitude.

high reduced frequencies, the variation of the lift deficiency function is very small, whereas at low reduced frequencies, the variation is high.[17] In other words, the behavior of the wake effect at low reduced frequencies is strongly nonlinear, whereas at high reduced frequencies, the behavior is approximately linear. As is known from classical theory, the wake effect in ground effect decreases compared to that of out of ground effect, as confirmed by the results (Fig. 14). Figure 14b shows contours of the first mode lift coefficient vs the ride height for various reduced frequencies. The behavior of the lift coefficient is nonlinear, but, similar to Fig. 14a, the differences between the curves remain approximately constant.

Following this discussion concerning the lift phase lag behavior, the lift amplitude behavior of the oscillating airfoil in ground effect for $k \rightarrow 0.0$ is also different than the behavior of the out of ground effect case. As the reduced frequency approaches zero, the aerodynamic forces of the oscillating wing in ground effect follow the corresponding forces for a fixed wing during a quasi-static airfoil motion. Because the aerodynamic forces are different at the instantaneous airfoil heights through the wing motion, a lift amplitude must exist. Note, this phenomenon is basically inviscid and is directly related to the lift phase lag behavior.

Streamwise Force of Oscillating Airfoils in Ground Effect

Results from the simulations of an oscillating airfoil in ground effect show that the streamwise force changes sign and that the value of the upper peak, namely, the drag, and the lower peak, namely, the thrust, are of the same order. Figure 15 shows the time history of two cycles of the force coefficient for two different reduced frequencies at various ride heights. The results presented follow the completion of one cycle of airfoil motion. Apparent from Fig. 15 is the presence of at least one additional frequency, especially at high reduced frequencies (Fig. 15b). Moreover, at a constant reduced frequency, a decrease in the ride height results in an increase to the streamwise force peaks with a higher increase of the lower peak. This means that higher thrust is expected with reducing ride heights. In addition, by

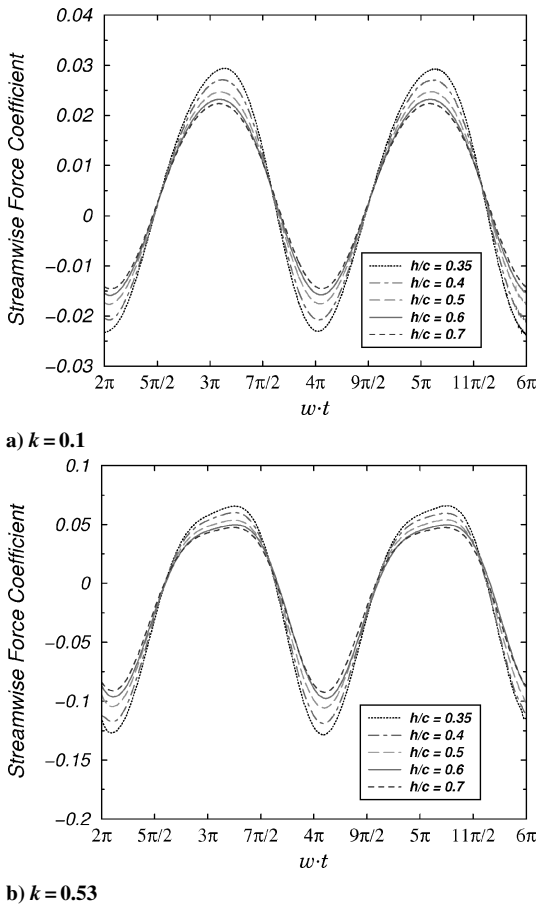

Fig. 15 Streamwise force coefficient time history in ground effect.

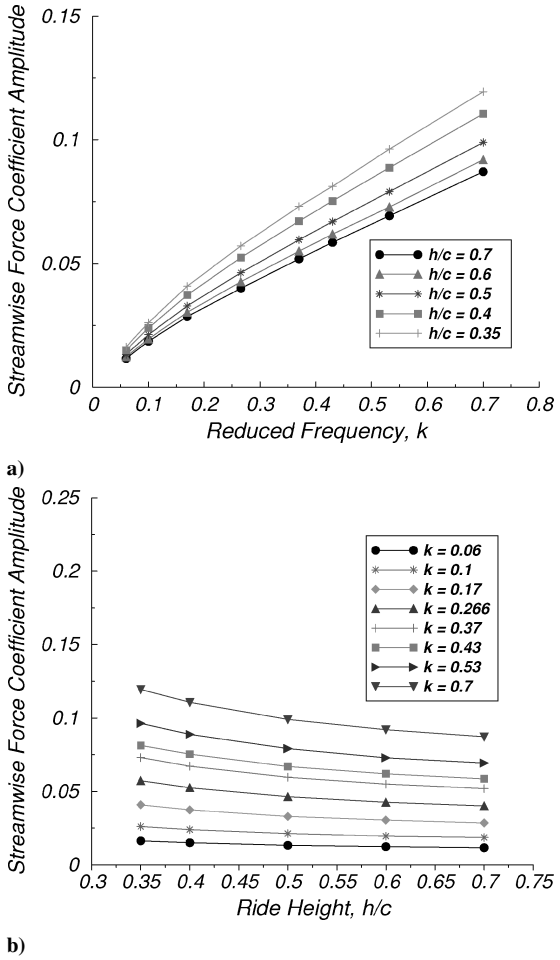

Fig. 16 First mode streamwise force coefficient amplitude.

comparison of the results for constant ride heights, one can see that an increase in the reduced frequency increases the force peaks with a higher increase of the lower peak. If one defines T as $T = -\bar{X}$, the total thrust, the higher increase of the lower peak also means that an increase of the reduced frequency is expected to increase the total thrust.

The results from the FFT analysis performed on the streamwise force in inviscid flow generally resemble the FFT results of the viscous flow. Figure 16 shows the general behavior of the first mode streamwise force in ground effect. Figure 16a shows plots of the streamwise force coefficient vs the reduced frequency for various ride heights. One can see that the streamwise force coefficient amplitude is nonlinear with the frequency and, in contrast to the behavior of the lift for this case, the differences between the curves do not remain constant. Figure 16b shows plots of the streamwise force coefficient vs the normalized height for various reduced frequencies. There is a resemblance to the behavior of the lift coefficient, and the differences between the curves remain approximately constant.

Qualitatively, the calculated streamwise force response of the oscillating airfoil is of a cosine shape. Under the assumption that unsteady aerodynamic effects can be neglected, the behavior of the force can be qualitatively explained as follows. By interpretation of the airfoil motion as an induced angle of attack, the coefficient of the instantaneous streamwise force acting on an airfoil undergoing a heaving motion in inviscid flow can be expressed as

$$C_X(t) = (\dot{H}/U_\infty)\left[\left(\alpha - \alpha_{l_0}\right) - \dot{H}/U_\infty\right]C_{l_\alpha} \tag{7}$$

where α_{l_0} is the zero-lift angle, α is the fixed angle of attack, $\dot{H}/U_\infty$ is the induced angle of attack, C_{l_α} is the lift coefficient slope, and $H = h + h_0 \sin(\omega t)$ is the harmonic oscillation motion function.

As discussed, an effective angle of attack, α_e, may be associated with each airfoil ride height. By substitution of the motion function

into Eq. (7) and by the use of the notion of effective angle of attack, the streamwise coefficient in ground effect may be expressed by

$$C_{X_{\text{aig}}}(t) = \omega(h_0/U_\infty)\cos(\omega t)\left[C_{l_{\alpha_e}}\alpha_e - C_{l_{\text{aog}}}\right] - \omega^2\left(h_0^2/U_\infty^2\right)\cos^2(\omega t)C_{l_{\alpha_e}} \quad (8)$$

where $C_{l_{\text{aog}}}$ is the lift out of ground effect and is equal to $C_{l_\alpha}\alpha_{l_0}$. Note that the last term in Eq. (8) is, in fact, the source of the second mode of the streamwise force.

For high ride heights, the term $(C_{l_{\alpha_e}}\alpha_e - C_{l_{\text{aog}}})$ is small, and, therefore, the streamwise force response is dominated by a squared cosine behavior. For low ride heights, this term becomes dominant, and, when accompanied by low frequencies, the streamwise force response is dominated by the cosine term. Note that a reduction in the ride height causes a nonlinear increase of the lift slope, which is the reason for the differences in the streamwise force coefficient slope at a constant ride height, as demonstrated in Fig. 16a. In the cases presented in the current work, the lift coefficient $C_{l_{\text{aog}}}$ is high, and, therefore, the cosine component of the streamwise force coefficient is more dominant.

According to the inviscid calculations, the total thrust in ground effect is positive for all reduced frequencies and ride heights. Figure 17 shows the logarithm of the total thrust coefficient vs the logarithm of the reduced frequency in and out of ground effect (Fig. 17a) and the variation of the thrust with ride height for various frequencies (Fig. 17b). The reduced frequency ranges between $0.17 < k < 0.7$. The logarithm of the total thrust in ground effect exhibits a linear dependence on the logarithm of the reduced frequency, namely $T \propto k^{C_0}$, where C_0 is a positive constant. Moreover, the slope of each of the curves corresponding to the various ride heights in ground effect is approximately the same (Fig. 17a). Note that the theoretical result of an airfoil out of ground effect can be approximated by a linear curve with a slope of 1.7, whereas the curve slope of the calculated results in ground effect is approximately 1.3. Similar to the thrust behavior out of ground effect, the thrust in ground effect increases with increasing reduced frequencies at a constant ride height. In addition, the thrust increases with reducing ride heights at constant reduced frequencies. The fact that the thrust at constant reduced frequencies increases with reducing ride heights is due to the reduction in the wake-induced velocity. It is, therefore, proposed here that for high frequencies, the total thrust in ground effect behaves as follows:

$$T_{\text{aig}}/T_{\text{aog}} \propto \exp[f(h/c)] \quad (9)$$

where $f(h/c)$ is a function of the airfoil ride height only.

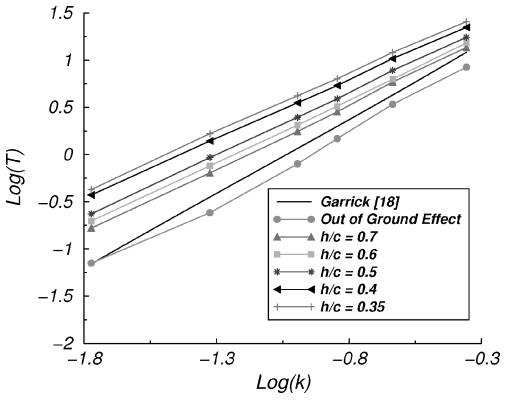

a)

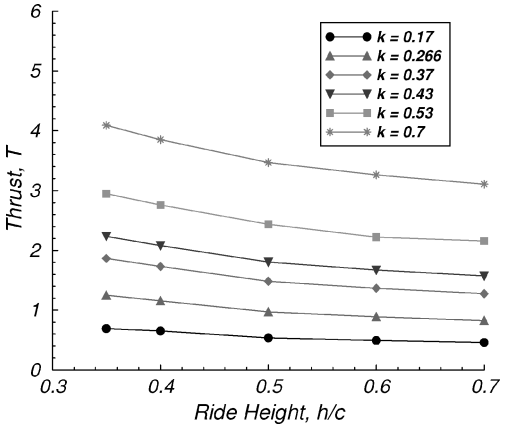

b)

Fig. 17 Thrust in ground effect.

Conclusions

The results presented for the fixed airfoil in extreme ground effect show significant differences between viscous flow simulations and inviscid flow simulations. The simulations that used the assumption of an inviscid flow predict higher levels of down-force compared to the viscous flow. This difference is amplified with reducing ride heights. Obviously, the inviscid flow simulations cannot predict the reduction in the down-force as predicted by the viscous flow simulations.

The generation of thrust by airfoil oscillations is basically an inviscid phenomenon. The results presented in this work show that in inviscid flows an increase in the reduced frequency or reduction in the ride height increases the total thrust. The most important result in this manner is the relation between the total thrust and the reduced frequency, namely, $T \propto k^{C_0}$. This result is consistent with the static case, $k \to 0.0$, where there is no thrust generation. The increasing total thrust with decreasing ride heights is also evident in viscous flows. However, the viscous flow simulations (Fig. 11) show that a positive total thrust is obtained only for sufficiently high frequencies. Nevertheless, the similar behavior between viscous and inviscid flows at high reduced frequencies confirms that the oscillatory motion is dominant at high reduced frequencies.

Another important result concerning the oscillating airfoil in inviscid flow is the behavior of the lift phase lag and amplitude. It is shown that at low reduced frequencies the aerodynamic forces follow the airfoil motion. That is, the lift phase lag approaches zero as the reduced frequency approaches zero. Consequently, the lift amplitude in this case is different than zero.

Acknowledgments

The authors acknowledge the use of computer resources belonging to the High Performance Computing Unit, a division of the Inter University Computing Center, which is a consortium formed by research universities in Israel. More information about this facility can be found at URL: http://www.hpcu.ac.il. The authors also thank the British American Racing Team and Willem Toet for providing the airfoil geometry, Gil Iosilevskii for hours of fruitful discussions, and Uri Goldberg for his assistance with implementing the turbulence model.

References

[1]Jones, K. D., Castro, B. M., Mahmoud, O., and Platzer, M. F., "A Numerical and Experimental Investigation of Flapping-Wing Propulsion in Ground Effect," AIAA Paper 2002-0866, Jan. 2002.

[2]Barber, T. J., Leonardi, E., and Archer, R. D., "Causes for Discrepancies in Ground Effect Analyses," *Aeronautical Journal*, Vol. 106, Dec. 2002, pp. 653–667.

[3]Knowles, K., Donoghue, D. T., and Finnis, M. V., "A Study of Wings in Ground Effect," *RAC Conference on Vehicle Aerodynamics*, Royal Aeronautical Society, London, 1994, pp. 22.1–22.13.

[4]Ranzenbach, R., and Barlow, J., "Two-Dimensional Airfoil in Ground Effect, An Experimental and Computational Study," Society of Automotive Engineers, SAE Paper 942509, 1994.

[5]Ranzenbach, R., and Barlow, J., "Cambered Airfoil in Ground Effect—Wind Tunnel and Road Conditions," AIAA Paper 95-1909, 1995.

[6]Ranzenbach, R., and Barlow, J., "Cambered Airfoil in Ground Effect—An Experimental and Computational Study," Society of Automotive Engineers, SAE Paper 960909, 1996.

[7]Chen, H. C., and Korpus, R., "A Multi-Block Finite-Analytic Reynolds-Averaged Navier–Stokes Method for 3-D Incompressible Flows," *ASME Summer Fluid Dynamic Conference*, American Society of Mechanical Engineers, Fairfield, NJ, 1993.

[8]Zerihan, J., and Zhang, X., "Aerodynamics of a Single Element Wing in Ground Effect," *Journal of Aircraft*, Vol. 37, No. 6, 2000, pp. 1058–1064.

[9]Zhang, X., and Zerihan, J., "Off-Surface Aerodynamic Measurements of a Wing in Ground Effect," *Journal of Aircraft*, Vol. 40, No. 4, 2003, pp. 716–725.

[10]Zerihan, J., and Zhang, X., "A Single Element Wing in Ground Effect; Comparisons of Experiments and Computation," AIAA Paper 2001-0423, Jan. 2001.

[11]Levy, Y., "Numerical Simulation of Dynamically Deforming Aircraft Configurations Using Overset Grids," *Journal of Aircraft*, Vol. 38, No. 2, 2001, pp. 349–354.

[12]Beam, R. M., and Warming, R. F., "An Implicit Factored Scheme for the Compressible Navier–Stokes Equations," *AIAA Journal*, Vol. 16, 1978, pp. 393–402.

[13]Steger, J. L., and Warming, R. F., "Flux Vector Splitting of the Inviscid Gasdynamics Equations with Applications to Finite-Difference Methods," *Journal of Computational Physics*, Vol. 40, 1981, pp. 263–293.

[14]Benek, J. A., Buning, P. G., and Steger, J. L., "A 3-D Chimera Grid Embedding Technique," AIAA Paper 85-1523, July 1985.

[15]Moryossef, Y., "A Computational Study of a Wing in Ground Effect," M.S. Thesis, Faculty of Aerospace Engineering, Technion—Israel Inst. of Technology, Haifa, Israel, June 2002.

[16]Goldberg, U., "Hypersonic Flow Heat Transfer Prediction Using Single Equation Turbulence Models," *Journal of Heat Transfer*, Vol. 123, 2001, pp. 65–69.

[17]Theodorsen, T., "General Theory of Aerodynamic Instability and the Mechanism of Flutter," NACA Rept. 496, 1934.

[18]Garrick, I. E., "Propulsion of a Flapping and Oscillating Airfoil," NACA Rept. 567, May 1936.

[19]Rozhdestvensky, K. V., and Ryzhov, V. A., "Aerohydrodynamics of Flapping-Wing Propulsors," *Progress in Aerospace Sciences*, Vol. 39, No. 8, 2003, pp. 585–633.

[20]Knoller, R., "Die Gesetze des Luftwiderstandes," *Flug-und Motortechnik (Wien)*, Vol. 3, No. 21, 1909, pp. 1–7.

[21]Betz, A., "Ein Beitrag zur Erklarung des Segelfluges," *Zeitschrift fur Flugtechnik und Motorluftschiffahrt*, Vol. 3, 1912, pp. 269–272.

[22]Katzmayr, R., "Effect of Periodic Changes of Angle of Attack on Behavior of Airfoils," NACA Rept. 147, 1922.

[23]Satyanarayana, B., and Davis, S., "Experimental Studies of Unsteady Trailing-Edge Conditions," *AIAA Journal*, Vol. 16, No. 2, 1978, pp. 125–129.

R. So
Associate Editor